A SUPERCONDUCTING ELECTRON SPECTROMETER

M. Guttormsen[+], H. Hübel, A.v. Grumbkow,
Y.K. Agarwal[++] and J. Recht

Institut für Strahlen- und Kernphysik,
Universität Bonn, D-5300 Bonn, West-Germany

K.H. Maier, H. Kluge, A. Maj[+++],
M. Menningen and N. Roy
Hahn-Meitner Institut für Kernforschung,
D-1000 Berlin, West-Germany

OUP -
Report 84-11 Received 16/3-1984

[+] Present address: Institute of Physics, University of Oslo, Oslo, Norway

[++] Present address: Tata Institute of Fundamental Research, Bombay, India

[+++] On leave from Institute of Nuclear Physics, Krakow, Poland.

2S/20.3.84

Abstract

The set-up and tests of an electron spectrometer for in-beam conversion electron measurements are described. A superconducting solenoid is used to transport the electrons from the target to cooled Si(Li) detectors. The solenoid is designed to produce either a homogeneous axially symmetric field of up to 2 Tesla or a variety of field profiles by powering the inner and outer set of coils of the solenoid separately. The electron trajectories resulting for various field profiles are discussed. In-beam electron spectra taken in coincidence with electrons, gammas and alpha-particles are shown.

1. Introduction

Conversion electron spectroscopy is an important method to determine multipolarities of γ-transitions. In some cases of low-energy and/or high multipolarity transitions in heavy nuclei it can even be the only method to detect these transitions. In "in-beam" measurements at accelerators, however, the huge background of low-energy δ-electrons, which is produced when the beam hits the target, makes the application of this method difficult. Usually only electrons above ~150 keV can be measured prompt with respect to the beam bursts of the accelerator. In the lower energy region, however, in many cases lifetimes of the deexciting states make it possible to discriminate electronically or by recoil-shadow methods against the prompt δ-electrons.

Several different types of β-spectrometers have been used for in-beam studies. In the spectrometers which magnetically focus electrons of definite energy onto a detector the field has to be stepped over the whole range of interest and measurements of conversion electron spectra can be quite time consuming. This disadvantage is avoided in spectrometers which use the magnetic field only to transport the electrons from the target to a detector which has to have good energy resolution for electrons. The discrimination against the low-energy δ-electrons can be achieved by baffle systems and/or by the applied magnetic field.

In this paper we describe the set-up of a spectrometer of the latter type. In principle our apparatus is similar to earlier spectrometers described in refs.[1-4]. However, it is the first system of this type in which a superconducting solenoid is applied to produce the transporting field for the electrons. In our spectrometer there is sufficient room between target and detector to reduce the background of γ-rays and neutrons produced in the nuclear reactions. It allows the measurement of electron -electron and γ-electron coincidences with high efficiency.

The spectrometer was developed in a collaboration between the University of Bonn and the HMI-Berlin. It was built and tested at the Bonn cyclotron, and is now installed on a beam line of the VICKSI accelerator facility of the HMI. Nearly identical systems have been installed by a group at LLNL, Los Alamos, and at the cyclotron of the KFA, Jülich.

In chapter 2 a description of the spectrometer is given and the cooling properties of the superconducting solenoid are discussed. The motion of electrons exposed to various magnetic field profiles is studied in chapter 3. In chapter 4 examples of results obtained in e^--e^-, e^--γ and e^--α coincidence measurements are given.

2. Description of the spectrometer

The β-spectrometer, as mounted on a VICKSI beam line, is shown in fig. 1. In the following we will limit the discussion on the most important aspects characterizing the present construction.

The superconducting solenoid was manufactured by Cryogenic Consultants Ltd., London. A sectional view of the solenoid with the liquid helium (ℓHe) reservoir is shown in fig. 2. The cylindrical vacuum chamber, in which electrons spiral along the magnetic field lines perpendicular to the beam direction has an inner diameter of 85 mm and a length of 650 mm. The ℓHe vessel mounted above the coils has a capacity of 3 ℓ. The helium cooled sections are surrounded by a ℓN_2 radiation shield (not shown in fig. 2) placed in the cryo-vacuum. The vacuum space for the target and the detectors is separated from the cryo-vacuum. Therefore one can freely work on the experimental set up while the magnet coils are cold.

Temperatures at different locations of the cryostat can be monitored during the cooling process and during the experiment. Two thermometers are connected to the ℓN_2 shield. Since the shield reduces the heat radiation, its temperature influences the He evaporation.

Thermometers are also connected to the parts of the spectrometer cooled by helium : one is mounted in the He reservoir (R), one at the long side (L) and one at the short side (S) of the solenoid. Fig. 3 displays the temperatures at these positions as a function of the cooling time. The He transfers were performed with a pressure of ~0.2 bar. The short side is cooled by heat conduction to the long side, and thus experiences the slowest cooling rate. It takes about six hours to cool from room temperature to 4.2 ^{o}K.

The amount of ℓHe in the reservoir is measured with a helium level gauge. The ℓHe holding time is ~7 h with field and ~9 h without field. If the magnets are switching from a superconducting to a normal state during operation (quenching) all ℓHe is blown out. After quenching the temperature is around 30 ^{o}K and a new ℓHe transfer is required. Typically, for a beam time of several days the ℓHe consumption amounts to ~100 liters.

The superconducting magnets (NbTi multicore filaments) consist of outer and inner coil pairs (see fig. 2). Each pair can be powered separately resulting in a variety of field profiles. Fig. 4 displays the axial magnetic field measured with a Hall probe on the axis of the solenoid. The measurements were performed with the maximum current of 62 A in the outer (upper part), the inner (middle part) and in both coil pairs (lower part). In the latter case an almost homogeneous field ($\Delta B/B \leq 3\%$) of 2T was obtained over a range of 500 mm. The coil arrangement is assymmetric with respect to the target position. The length of the short side allows for instance to insert a Ge detector to measure γ-rays and provides easy access to the target area, while the long side is optimized for measuring electrons.

The ℓN_2 cooled Si(Li) electron detectors are mounted on cold fingers which are attached to ℓN_2 dewars (see fig. 2). Long bellows permit to

position the detectors at the appropriate distance from the target or to withdraw the detectors and disconnect the detector and target chamber vacuum.

The Si(Li) detectors used in the first experiments have an active area of 300 mm^2 and a sensitive depth of 2 mm (manufactured by Schlumberger). The surface of the detectors can easily be damaged by small amounts of oil and other deposits. Therefore, the main chamber inside the solenoid is evacuated by a cryo-pump to ensure a clean and good vacuum.

The Si(Li) detectors are kept at room temperature when not in use. Immediately before cooling, they are pumped with the cryo-pump. In this way the surface of the Si(Li) detectors are to some extent cleaned before the cooling process starts. About 3 h after the dewar is filled with ℓN_2, high voltage can be applied. Our Si(Li) detectors have gone through several cycles of cooling and warming in the past two years and so far no deterioration is observed. The Si(Li) detectors were found to work well in the magnetic field: At the highest field of B = 2 T the resolution was reduced only by 20%.

On the short side the Si(Li) detector can be replaced by a longnosed Ge detector to measure γ-rays from the target. This is a very efficient set-up for measuring coincidences between γ-rays and electrons, which are detected on the long side. Tests with various Ge(Li) detectors revealed problems with Penning effects. The behaviour of a n-type Ge counter (ORTEC gamma-X) specially designed for magnetic fields is shown in fig. 5. Still, in this case the resolution (FWHM and FWTM) is impaired by the magnetic field.

Fig. 6 displays a cross section perpendicular to the solenoid axis. The vacuum chamber has three rectangular windows around the target; each of 30 mm width and 230 mm length.At the lower window the target sluice

is mounted. Using a valve and separate pumping facilities targets can be changed without breaking the main vacuum. The sluice including target-rod and target can be moved in the direction of the beam by remote control over a distance of 20 mm for recoil-distance measurements.

On its way through the solenoid the incident beam will be deflected by the magnetic field. Fortunately, the deflection in the fringe fields outside the magnet compensates the deflection caused by the field in the inside. Hence, the position of the beam on the target does not change appreciably when the field is varied; as illustrated in fig. 6. However, the angle at which the beam hits the target does depend on the magnitude of the field. This angle is important in recoil-shadow measurements[4] and the solenoid can therefore be tilted by $\pm 30^{\circ}$ around its symmetry axis. The spectrometer mount also provides for an adjustment of its height. A flexible connection to the beam line allows both movements. As the electron spectrometer is mainly used for heavy-ion beams the beam is dumped directly in a lead Faraday cup situated behind the target. The heavy ion beam may show a wide distribution of charge states after passing the target and spreads out in the magnetic field. By appropriately tilting the spectrometer the bulk of the beam is guided into the Faraday cup.

3. Field profiles and electron orbits

The separate operation of the two coil pairs makes it possible to choose field profiles appropriate for each experimental set-up. In the following, we will describe the motion of electrons for three types of profiles and discuss the parameters of experimental relevance.

In a homogeneous field the electrons move on helical paths with a constant velocity component

$$v_z = |\bar{v}| \cos\theta \qquad (1)$$

along the symmetry axis of the solenoid (for symbols, see fig. 7). The orbital radius is given by

$$\rho = ((B\rho)_E/B)\cos\theta \ . \qquad (2)$$

The Bρ-value for electrons with kinetic energy E reads approximately

$$(B\rho)_E = 0.3334[2(mc^2)E + E^2]^{\frac{1}{2}} \ , \qquad (3)$$

where Bρ and E are expressed in units of Tesla x cm and MeV, respectively. Homogeneous fields have been successfully used in the so-called lens mode and recoil shadow method and have been extensively discussed in ref.[4]. The lens mode has been developed and used for an identical spectrometer by a group at LLNL[5], and will not be discussed further in this article.

For fields with more complicated profiles (as e.g. shown in figs. 8 and 9) the electron trajectories have to be calculated by numerical integration. In this work we have used a computer code[6] which calculates the magnetic field from the geometry of the coils and the current and integrates the equations of motion. For many applications the adiabatic approximation is sufficient to describe the electron motion by the following formulas which relate the average orbit parameters at two different positions along the symmetry axis

$$(B_1/B_2)^{\frac{1}{2}} = \frac{\sin\theta_1}{\sin\theta_2} = \frac{\rho_2}{\rho_1} = \frac{r_2}{r_1} \ . \qquad (4)$$

θ, ρ and r are the angle with the symmetry axis, the radius of the orbit, and the distance of the spiral from the symmetry axis, respectively.

When the current in the inner coils exceeds the current in the outer pair of coils ($I_{inner} > I_{outer}$) a <u>bump</u> appears in the field profile

at the target position ($z = 0$). This situation is shown in fig. 8 where $I_{inner} = 2I_{outer} = 62$ A. The figure includes the trajectory of a 100 keV electron leaving the target ($z = 0$) at $r = 0.5$ cm and with $\theta = 25^{o}$. On its way from target to detector ($z \sim 35$ cm) the electron experiences about 70 revolutions with orbital diameters ranging from 0.5 mm ($z = 0$) to 0.7 mm ($z \sim 35$ cm). It is interesting to notice that the electron spirals gradually to a larger distance r from the symmetry z-axis. Here, the electron roughly follows the field lines which are diverging with decreasing field. If $I_{inner} >> I_{outer}$ it might happen that r becomes larger than the radius of the detector (1 cm) and the electron thereby escapes detection.

The type of field profile shown in fig. 8 makes the motion of the electrons more forward directed with increasing z. Using eq. (4) with $B_1(z = 0) \sim 1.6\ B_2(z \sim 35\ cm)$ electrons starting at $\theta_1 \sim 90^{o}$ hit the detector with $\theta_2 \sim 52^{o}$. This reduces the number of backscattered electrons from 65% to 48% according to the estimates of Waldschmidt and Wittig[7]. The probability of depositing full energy is further increased by the fact that some of the backscattered electrons will be reflected into the detector by the rising field. Clearly for this field shape both detectors have a solid angle of $\sim 2\pi$.

Another interesting consequence of eq. (4) is the magnetic mirror effect. For $\theta_2 = 90^{o}$ the electron will no longer move towards the detector. This situation occurs for an initial angle θ_1 given by

$$\theta_{refl} = \arcsin[(B_1/B_2)^{\frac{1}{2}}] \quad . \tag{5}$$

Figure 9 displays a field profile with a dip in the center. Here, electrons will be reflected for initial angles $\theta_1 > \theta_{refl} = 33^{o}$ at a distance of $z = 21$ cm from the target. For $\theta_1 = 55^{o}$ e.g. the trapped electrons will spiral in between $z = -7$ cm and $+7$ cm and slowly drift off in radial direction. The mirror effect can be applied to discriminate

certain initial angles and thereby obtain information about the angular distribution.

The calculated electron trajectory of fig. 9 shows that the average distance to the symmetry z-axis decreases with increasing z. This feature can be utilized as a focusing mechanism in cases where the electrons are emitted far away from the z-axis.

4. Measurements

The in-beam performance of the spectrometer was tested in several nuclear reactions using various field profiles and baffle systems. The results from some experiments have already been reported.

Delayed e^--e^- coincidences were measured for several Hg isotopes using (α,4n) and (^{14}N,5n) reactions. Fig. 10 illustrates the experimental set-up where two semicylindrical baffles were used. The evaporation residues recoiled out of the thin target which was placed ~2 mm behind the edge of the baffles. The magnetic field was chosen high (B = 1.4 T) in the target area resulting in electron orbit radii (eq. (2)) of e.g. ρ(20 keV) = 0.34 mm and ρ(200 keV) = 1.2 mm. Hence, the baffle system could discriminate effectively against prompt electrons, in particular against δ-electrons. Since only conversion electrons from recoiling nuclei could be detected, the spectra were almost background free as is evident in fig. 11. For the chosen set-up (fig. 10) both the $12^+ \rightarrow 10^+$ (52 keV) as well as the $8^- \rightarrow 7^-$ (228 keV) transitions are detected with high coincidence efficiency despite their different lifetimes ($T_{\frac{1}{2}}$ = 8.1(5)ns and 0.912(30) ns, respectively, see refs.[8,9]). Further details on this e^--e^- coincidence experiment are given elsewhere[10]. Other examples of the use of the spectrometer in this configuration are presented in a study of the ^{203,205}Bi isotopes[11] and of the ^{215}Fr nucleus[12].

An example for conversion electron X-ray coincidences in the β-decay of ^{213}Ra is shown in fig. 12. The nucleus ^{213}Ra has a 20% K capture

branch to ^{213}Fr and a half-life of $T_{\frac{1}{2}} = 2.7$ m. It was produced by the $^{204}Pb(^{13}C,4n)^{213}Ra$ reaction. The reaction products recoiled out of the thin target and were stopped in 500 $\mu g/cm^2$ carbon foils. The foils were transported by a belt into the spectrometer for the measurements. A Si(Li) detector for electrons on the long side and a gamma-X-ray counter for γ-rays about 3 cm from the foils on the short side were used. The e^--X-ray coincidences occur predominantly with the X-ray emitted as a consequence of a K-converted transition. Therefore, mainly K-conversion lines of francium nuclei are seen in the coincident electron spectrum. This simplifies the spectrum so that it may be compared to a γ-spectrum from a chemically separated source. A further advantage is the absence of the Compton continuum in the spectra. Particularly in decay studies conversion electrons are important to determine multipolarities of transitions, since angular correlation measurements of γ-rays are very tedious.

Finally fig. 13 shows α-e^--coincidences in the decay of $^{217}Ac^m$. This isomer was produced in a thin ^{209}Bi target inside the spectrometer, located 3 cm in front of the symmetry axis, by the $^{209}Bi(^{12}C,4n)$ reaction. Shadows-baffles prevented electrons from the target to reach the Si(Li)-detectors on both sides of the solenoid. The actinium nuclei left the target and were stopped in a thin aluminium foil on the spectrometer axis, while the bulk of the beam passed through a hole in this catcher foil. The foil was also viewed by two α-detectors at $\pm 135^\circ$ to the beam with a solid angle of ~0.4 sr. As is evident from the decay scheme shown in fig. 13, electrons which are delayed with respect to the pulsed beam and followed by a coincident α-particle from the very fast α-decay of the ground state, have to be emitted in the decay of $^{217}Ac^m$. These transitions are seen in fig. 13. This spectrum and simultaneously measured e^--e^--coincidences gave the information on the highly converted low

energy transitions which was lacking from γ-ray spectroscopy and was needed to establish the decay scheme.

In the experiments described above we have used the spectrometer in the broad range mode for coincidence studies of delayed conversion electrons. It is particularly useful in this mode of opeartion due to the large solid angle and since the whole energy range is measured at once. The overall time resolution in e^--e^--coincidences with a treshold of 30 keV is Δt(FWHM) = 100 to 200 ns. The prompt δ-electrons from the target were always prevented from reaching the detectors by shadows. Two short trials to measure prompt electrons have not been successful due to the very strong δ-electron background with heavy ion beams. For this type of application schemes as used by Goerlach et al[13] can and have to be used here too.

5. Advantages and disadvantages of the superconducting solenoid

The advantages of this superconducting solenoid is that one reaches 3 to 4 times the magnetic field of a normal conducting version. Therefore, the electron orbit radii can be kept small compared to the detector radius for the energy range of interest ($\lesssim$ 2 MeV), and the detection efficiency is practically independent of energy. In the recoil shadow mode shorter lifetimes can be measured as the limit is determined by ρ/v_n, where v_n is the velocity of the recoiling nucleus. The main benefit is, however, that the field can vary by a factor of 5 or even 10 between the target and the detector and still be large enough at its minimum. In other words we can select the field strength at the target and at the detector (by its position) and the general field shape quite independent of each other. Thereby we can e.g. limit the acceptance in angle by the mirror effect to reduce line broadening due to Doppler shifts, if the electrons are emitted by nuclei in flight. Simultaneously

the path length of these nuclei from which electrons reach the detector can be adjusted as required. The increased space around the target makes it possible to install e.g. additional detectors with ease adding much to the possibilities of the instrument.

The use of the equipment is about as convenient as for a normal conducting version. Quenching of the superconducting coils is rare due to the conservative design. In general one only has to expect one quench after moving the spectrometer and it then takes about ½ hour to get back into operation. The inconvenience of handling liquid nitrogen and helium balances that of high power with a big supply, thick cables and cooling water hoses. The running costs are also comparable. The time for cooling down of approximately one working day and the need to refill liquid helium, due to the small reservoir, every 8 hours are somewhat cumbersome.

Acknowledgement

The authors would like to thank D. Rosendaal for his help in the construction of the spectrometer. Discussions with our collegues at LLNL and Jülich who installed identical systems were very helpful. For the design of the spectrometer we profited much from the experience of H. Backe and U. Goerlach.

This work was supported by the Minister für Forschung und Technologie of the Federal Republic of Germany and by the Ministerium für Wissenschaft und Forschung des Landes Nordrhein-Westfalen.

References

1. K. Kotajima and R. Beringer, Rev.Sci.Instr. 41 (1970) 632

2. Th. Lindblad and C.G. Lindén, Nucl.Instr. and Methods 126 (1975) 397

3. J. Konijn, W.L. Posthumus, P.F.A. Goudsmit, C. Schiebaan, H.P. Geerke, J.L. Maarleveld, J.H.S. Andringa and G.J. Evers, Nucl.Instr. and Methods 129 (1975) 167

4. H. Backe, L. Richter, R. Willwater, E. Kankeleit, E. Kuphal, Y. Nakayama and B. Martin, Z.Phys. A285 (1978) 159

5. J. Kantele, W. Stöffl, L.E. Ussery, D.J. Decman, E.A. Henry, R.W. Hoff, L.G. Mann and G.L. Struble, Phys.Rev.Lett. 51 (1983) 91.

6. R. Guenther, R.M. Schmidt, C. Vidic, Wissenschaftlicher Ergebnisbericht HMI-376 (1981), Bereich Datenverarbeitung und Elektronik, HMI Berlin.

7. M. Waldschmidt and S. Wittig, Nucl.Instr. and Methods 64 (1968) 189

8. R. Kroth, thesis, Bonn University (1981)

9. C. Günther, H. Hübel, A. Kleinrahm, D. Mertin, B. Richter, W.D. Schneider and R. Tischler, Phys.Rev. C15 (1977) 1298

10. M. Guttormsen, A. von Grumbkow, Y.K. Agarwal, K.P. Blume, K. Hardt, H. Hübel, J. Recht, P. Schüler, H. Kluge, K.H. Maier, A. Maj and N. Roy, Nucl,Phys. A398 (1983) 119

11. H. Hübel, M. Guttormsen, K.P. Blume, J. Recht, A.v. Grumbkow, K. Hardt, P. Schüler, Y.K. Agarwal and A. Maj, Z.Physik A314 (1983) 89.

12. D.J. Decman et al., Nucl.Phys. A, in press.

13. U. Goerlach, D. Habs, V. Metag, B. Schwartz, H.J. Specht and H. Backe, Phys.Rev.Lett. 48 (1982) 1160.

Figure captions

Fig. 1 The β-spectrometer installed at a beam line at the Hahn-Meitner-Institut, Berlin.

Fig. 2 The superconducting solenoid with ⁴He reservoir and one Si(Li) electron detector.

Fig. 3 The temperature as function of time during the cooling with liquid nitrogen (upper curves) and liquid helium (lower curves).

Fig. 4 Magnetic fields measured along the solenoid axis with a current of 62A in the outer, inner and both coil pairs.

Fig. 5 The resolution at 1.3 MeV γ-ray energy for a γ-X-ray (ORTEC) Ge detector as function of external magnetic field.

Fig. 6 Cross-section of the spectrometer mounted at the beam line; it is tilted by 20° in order to compensate for the beam bending.

Fig. 7 The coordinates describing an electron with velocity vector $\vec{v}$ at an angle θ to the solenoid symmetry z-axis. The distance to the z-axis is denoted by r.

Fig. 8 The motion of a 100 keV electron in the long side of the solenoid starting with $z = 0$, $r = 0.5$ cm and $\theta = 25^{\circ}$. The electron is exposed to a field obtained with 62A and 31A in the inner and outer coil pairs, respectively.

Fig. 9 The motion of a 100 keV electron starting at $z = 0$, $r = 0.5$ cm and $\theta = 20^{\circ}$. The field is produced with 62A in the outer coil pair.

Fig. 10 Set-up used in the delayed e^{-}-e^{-} coincidence experiment. Evaporation residues were allowed to recoil out of the thin target which was placed behind the baffles in order to discriminate against prompt electrons.

Fig. 11 Electron-electron coincidence spectra of ^{194}Hg with gates on the $8^- \rightarrow 7^-$ (upper part), the $7^- \rightarrow 5^-$ (middle part) and the $10^+ \rightarrow 8^+$ transitions (lower part) [ref.[10]].

Fig. 12 K-conversion electrons in coincidence with K_α X-rays from francium in the ^{213}Ra EC ^{213}Fr decay. Note that only K-lines appear in the spectrum.

Fig. 13 Conversion electrons in coincidence with α-particles of $E_\alpha = 9.65$ MeV from the $T_{1/2} = 69(4)$ ns decay of the ^{217}Ac ground state.

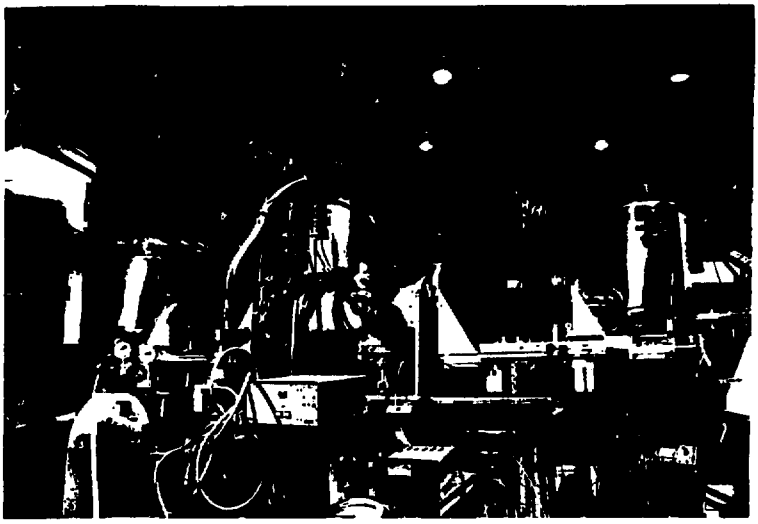

Fig 1

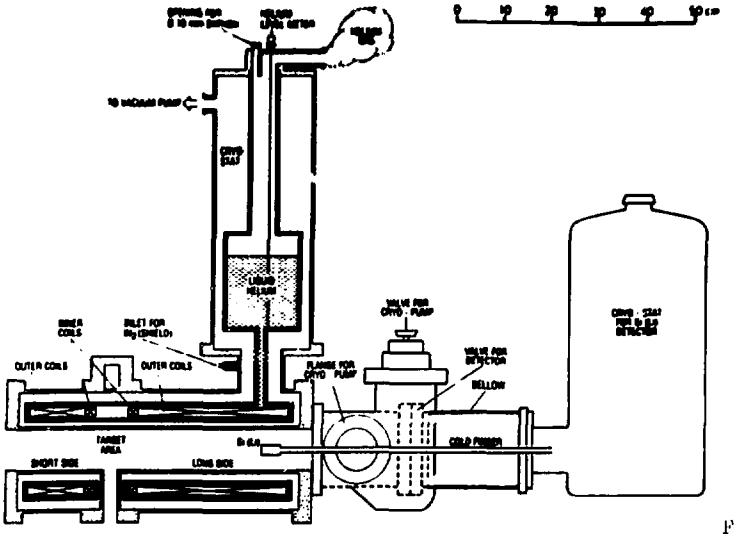
0 10 20 30 40 50 cm
10 MICRON PUMP
CRYO STAT
LIQUID HELIUM
VALVE FOR CRYO - PUMP
VALVE FOR DETECTOR
BELLOW
CRYO - STAT FOR H.F. DETECTOR
INNER COILS
OUTER COILS
OUTER COILS
FLANGE FOR CRYO PUMP
TARGET AREA
SHORT SIDE
LONG SIDE
COLD FINGER

Fig 2

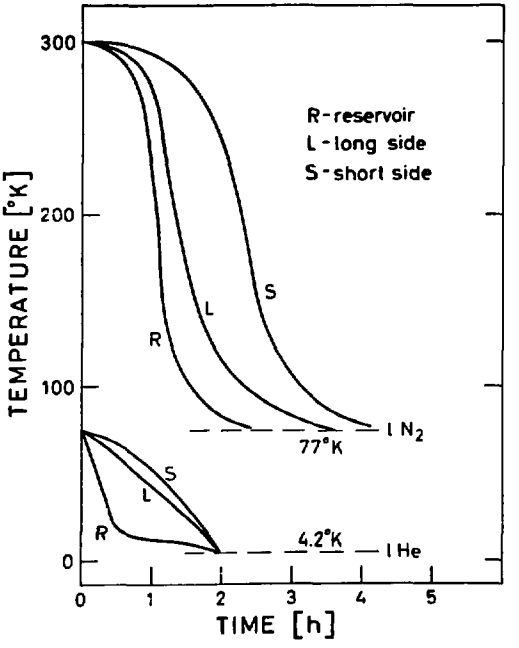
300
200
100
0
TEMPERATURE [°K]
R-reservoir
L-long side
S-short side
S
L
R
l N2
77°K
S
L
R
4.2°K
l He
0
1
2
3
4
5
TIME [h]

Fig 3

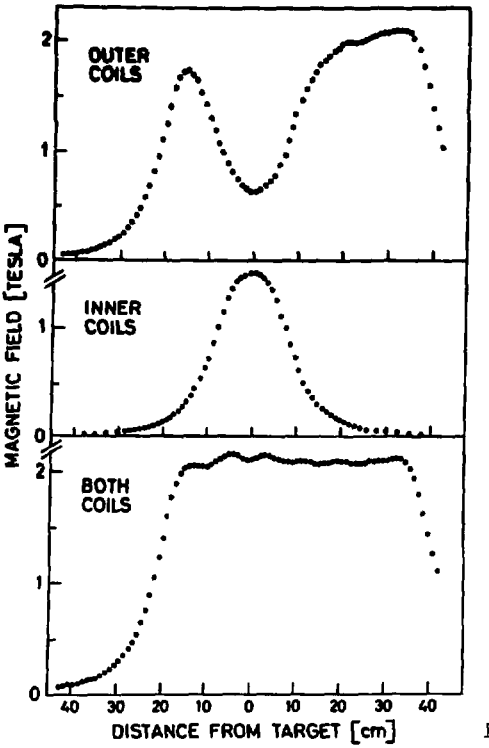
OUTER COILS
INNER COILS
BOTH COILS
MAGNETIC FIELD [TESLA]
DISTANCE FROM TARGET [cm]
2
1
0
40
30
20
10
0
10
20
30
40

Fig 4

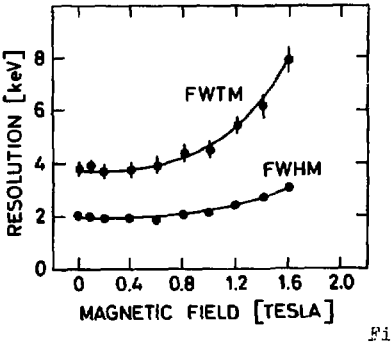
FWTM
FWHM
RESOLUTION [keV]
MAGNETIC FIELD [TESLA]
8
6
4
2
0
0
0.4
0.8
1.2
1.6
2.0

Fig 5

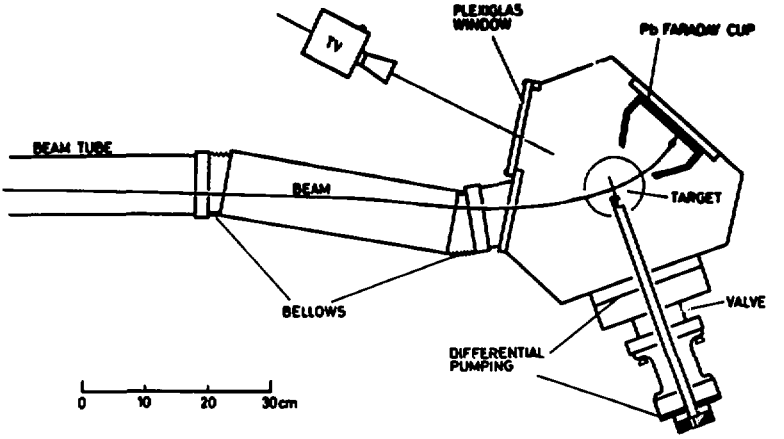
PLEXIGLAS WINDOW
Pb FARADAY CUP
BEAM TUBE
BEAM
TARGET
BELLOWS
VALVE
DIFFERENTIAL PUMPING
0
10
20
30cm

Fig 6

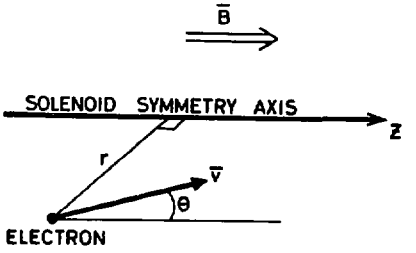
B
SOLENOID SYMMETRY AXIS
z
r
v
θ
ELECTRON

Fig 7

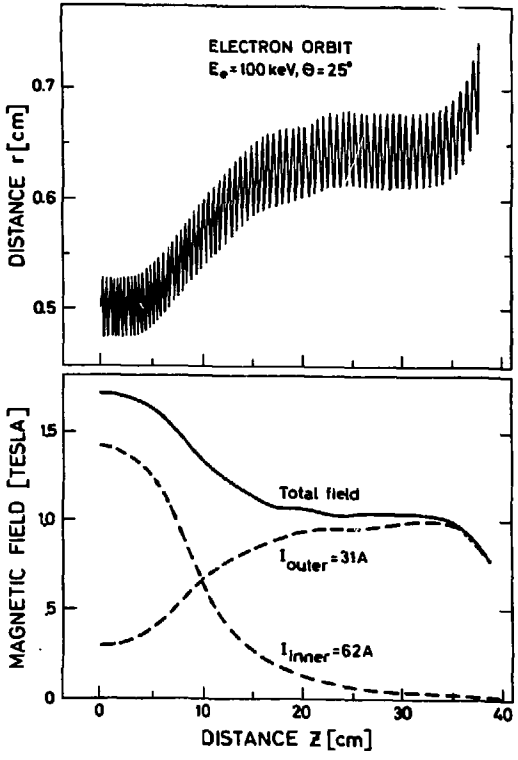
ELECTRON ORBIT
E_e = 100 keV, Θ = 25°
DISTANCE r [cm]
0.7
0.6
0.5
MAGNETIC FIELD [TESLA]
Total field
I_{outer} = 31A
I_{inner} = 62A
0
10
20
30
40
DISTANCE Z [cm]

Fig 8

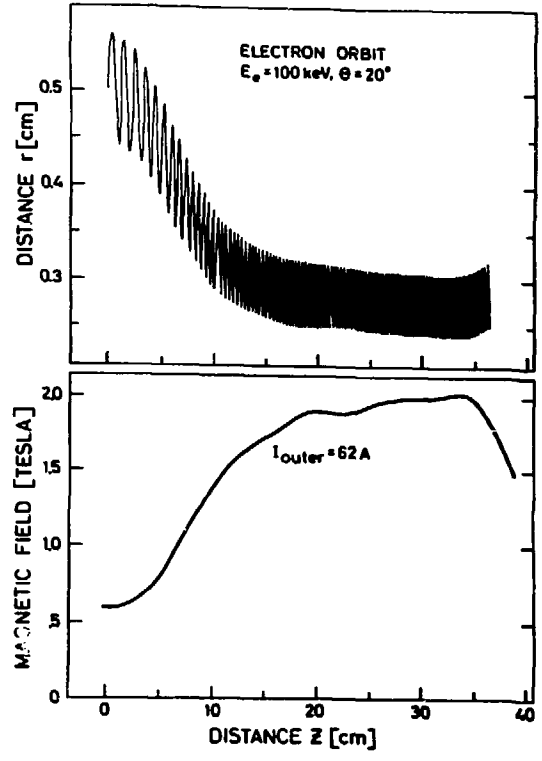
ELECTRON ORBIT
E_e = 100 keV, Θ = 20°
DISTANCE r [cm]
0.5
0.4
0.3
MAGNETIC FIELD [TESLA]
I_{outer} = 62A
2.0
1.5
1.0
0
10
20
30
40
DISTANCE Z [cm]

Fig 9

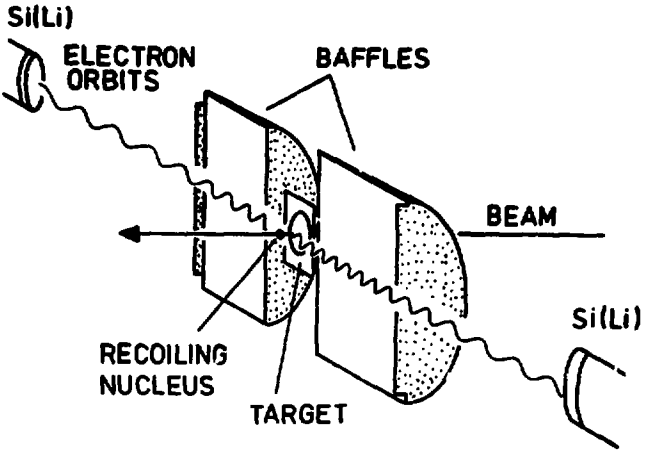
Si(Li)
ELECTRON ORBITS
BAFFLES
BEAM
Si(Li)
RECOILING NUCLEUS
TARGET

Fig 10

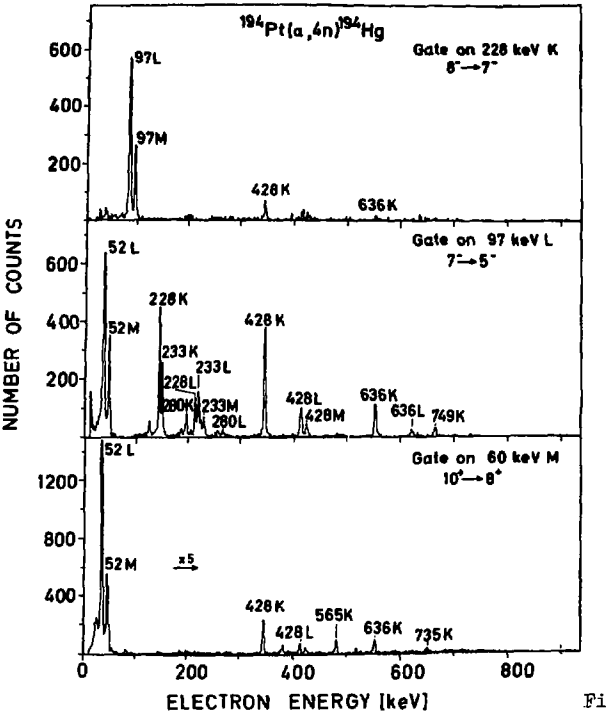
^{194}Pt(α,4n)^{194}Hg
Gate on 228 keV K
8⁻→7⁻
97L
97M
428K
636K
Gate on 97 keV L
7⁻→5⁻
52L
52M
228K
233K
233L
228L
280K
233M
280L
428K
428L
428M
636K
636L
749K
Gate on 60 keV M
10⁺→8⁺
52L
52M
x5
428K
428L
565K
636K
735K
NUMBER OF COUNTS
ELECTRON ENERGY [keV]

Fig 11

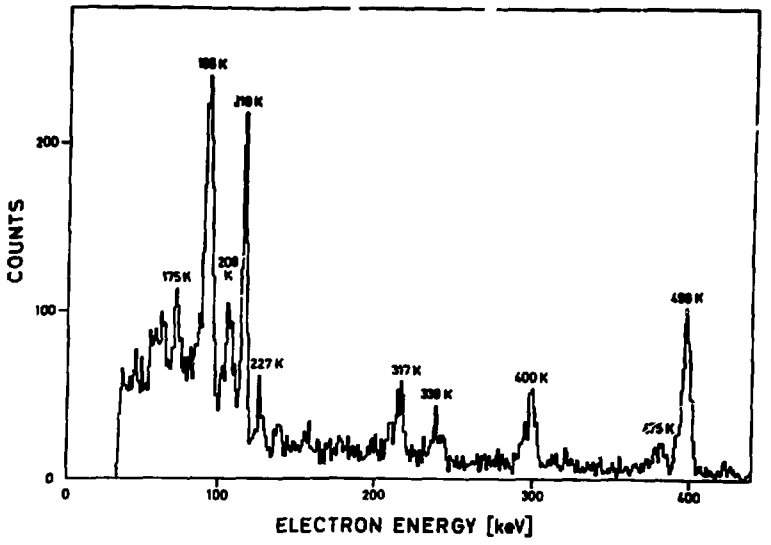
COUNTS
ELECTRON ENERGY [keV]
175 K
208 K
227 K
317 K
338 K
400 K
498 K

Fig 12

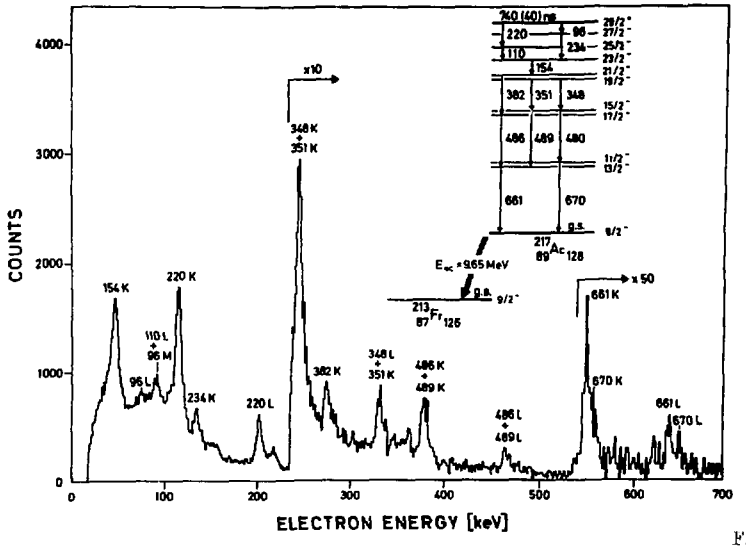
COUNTS
ELECTRON ENERGY [keV]
154 K
220 K
110 L + 96 M
96 L
234 K
220 L
x10
348 K + 351 K
382 K
348 L + 351 K
486 K + 489 K
486 L + 489 L
x50
681 K
670 K
661 L
670 L
240 (40) ns
220
110
154
382
351
348
486
489
480
661
670
g.s.
$^{217}_{89}Ac_{128}$
$E_{\alpha c}$ = 9.65 MeV
$^{213}_{87}Fr_{126}$

Fig 13